Rupture process of liquid bridges: The effects of thermal fluctuations

Jiayi Zhao,[1] Nan Zhou,[2] Kaixuan Zhang,[2] Shuo Chen,[2,*] Yang Liu,[3] and Yuxiang Wang[4]

[1]*School of Energy and Power Engineering, University of Shanghai for Science and Technology, Shanghai 200093, China*
[2]*School of Aerospace Engineering and Applied Mechanics, Tongji University, Shanghai 200092, China*
[3]*Department of Mechanical Engineering, The Hong Kong Polytechnic University, Hung Hom, Hong Kong, China*
[4]*Department of Chemical Engineering, Monash University, Clayton, Victoria 3800, Australia*

(Received 15 January 2020; accepted 31 July 2020; published 31 August 2020)

Rupture of a liquid bridge is a complex dynamic process, which has attracted much attention over several decades. We numerically investigated the effects of the thermal fluctuations on the rupture process of liquid bridges by using a particle-based method know as many-body dissipative particle dynamics. After providing a comparison of growth rate with the classical linear stability theory, the complete process of thinning liquid bridges is captured. The transitions among the inertial regime (I), the viscous regime (V), and the viscous-inertial regime (VI) with different liquid properties are found in agreement with previous work. A detailed description of the thermal fluctuation regime (TF) and another regime, named the breakup regime, are proposed in the present study. The full trajectories of thinning liquid bridges are summarized as I → V → VI → TF → breakup for low-Oh liquids and V → I → Intermediate → V → VI → TF → breakup for high-Oh liquids, respectively. Moreover, the effects of the thermal fluctuations on the formation of satellite drops are also investigated. The distance between the peaks of axial velocity is believed to play an important role in forming satellite drops. The strong thermal fluctuations smooth the distribution of axial velocity and change the liquid bridge shape into a double cone without generating satellite drops for low-Oh liquids, while for high-Oh liquids, this distance is extended and a large satellite drop is formed after the breakup of the liquid filament occurs on both ends, which might be due to strong thermal fluctuations. This work can provide insights on the rupture mechanism of liquid bridges and be helpful for designing superfine nanoprinting.

DOI: 10.1103/PhysRevE.102.023116

I. INTRODUCTION

Due to surface-tension-driven instability, a long liquid bridge tends to spontaneously decay into drops. This ubiquitous phenomenon has attracted great attention because of its importance for many potential applications, including superfine nanoprinting [1,2], nanoscale manufacture [3], DNA arraying [4,5], reagents transport [6], etc. The vast prospects for these applications appeal for the further understanding of the breakup dynamics of liquid bridges. The pioneering studies concerning instability of liquid bridges date back more than a century; these were proposed by Plateau [7] and Rayleigh [8], respectively. They provided a stability analysis to illustrate that an indefinitely long liquid jet would pinch off if its circumference is smaller than the wavelength of perturbation. The competition between surface tension and inertia plays a key role in the breakup dynamics for liquid bridges according to Rayleigh's research. The famous Navier-Stokes equations are required to be solved accurately to understand the thinning mechanism of liquid bridges. Unfortunately, these three-dimensional nonlinear equations are hopelessly complicated and time consuming [9]. Alternatively, the three-dimensional Navier-Stokes equations were simplified into a one-dimensional model by adopting the lubrication approximation [10]. If the variations along the liquid bridge are slow and the liquid bridge is sufficiently slender, the variables in the transversal direction can be described as a simple function which only depends on the axial coordinate and time. The amount of computation is significantly reduced under this assumption. Besides with lubrication approximation, the self-similar theory [11] was also introduced to avoid the singularity of Navier-Stokes equations near the pinch point. The length scale of the solution now solely relies on time until the liquid bridge breaks up. The scaling number α has been widely investigated by theoretical and experimental analysis [12–20]. There are three main regimes during the thinning process, namely, inertial regime (I), viscous regime (V), and viscous-inertial regime (VI). They are influenced by the Ohnesorge number (Oh) as

$$\mathrm{Oh} = \frac{\mu}{\sqrt{\rho\sigma R_0}}, \tag{1}$$

where Oh is the ratio between viscous length $l_v = \mu^2/\rho\sigma$ and characteristic length R_0 of the system which is chosen as the radius of the original liquid bridges. The three main regions for a thinning liquid bridge are illustrated as follows.

A. Inertial regime (I)

If fluids are nearly inviscid, i.e., $\mathrm{Oh} \ll 1$, the viscous effect can be ignored and the balance between inertial and

*schen_tju@tongji.edu.cn

surface tension determines the deformation of the interface. The pinch-off is caused by the principal curvatures through the mean curvature, which is described by the Young-Laplace equation. A special feature of regime I is the overturning of the free surface, which has been studied both by experiments and simulations [12,13]. The double-cone shape is formed when the liquid bridge breaks up and the angles are predicted as 18.1° and 112.8°, respectively. In a self-similar theory, the scaling relation between the minimal radius of the liquid filament $h_{\min}$ and time is found in regime I as [14–16]

$$\frac{h_{\min}}{R_0} \propto \tau^{2/3}, \tag{2}$$

where τ is normalized by t_I, which is the characteristic pinch-off time in the I regime as $t_I = \sqrt{\rho R_0/\sigma}$, and is defined as $\tau = t_0 - t/t_I$. t_0 is the breakup time.

B. Viscous regime (V)

On the contrary, when Oh $\gg 1$, the viscous effect dominates the dynamics of the liquid bridges. Navier-Stokes equations are approximate to one dimension which depends on the assumption of a long slender bridge. In the V regime, symmetrical and asymmetrical rupture processes can be captured; meanwhile, squeezing and the pinch-off stage are investigated respectively [17]. Now a similar solution is achieved by Stokes flow as [18,19]

$$\frac{h_{\min}}{R_0} \propto \tau^1. \tag{3}$$

C. Viscous-inertial regime (VI)

However, the local Reynolds number $\mathrm{Re}_{\mathrm{local}}$ is close to zero and infinite if the liquid bridges approach pinch-off in theoretical analysis for the I and V regimes, which is contradictory and unphysical. Hence these two regimes are believed to be not able to depict the whole process to breakup. A regime where the effects of viscosity, inertia, and capillarity are balanced should be considered [20]. In the VI regime, $\mathrm{Re}_{\mathrm{local}} \sim 1$ is satisfied and α is the same as that in the V regime and a highly asymmetric interface shape joining a thin thread to a droplike profile is the special feature.

D. Regime transitions

Due to the existence of the VI regime, the transition from the I to the VI regime or from the V to the VI regime is unavoidable and takes place at small scale. It is very important to understand these transitions during the thinning process. According to the assumption of $\mathrm{Re}_{\mathrm{local}} \sim 1$, the transition occurs when [21,22]

$$\frac{h_{\min}}{R_0} \propto \mathrm{Oh}^2(\mathrm{I} \to \mathrm{VI}), \quad \frac{h_{\min}}{R_0} \propto \mathrm{Oh}^{-3.1}(\mathrm{V} \to \mathrm{VI}). \tag{4}$$

However, a recent study presented by Castrejón-Pita *et al.* showed that the transition may be more complex as described above [23]. They found a number of intermediate regimes in the process of filament thinning by using the Galerkin–finite-element method and experimental measurements. These intermediate regimes delay the onset of the final VI regime. The additional V regime was discovered for low-Oh liquids, suggesting that viscous force would dominate the thinning process even though the Oh number is quite small. Similarly, the presence of the I regime for high-Oh liquidds was thought to be the reason for the formation of satellite drops. Castrejón-Pita's work enriches our understanding of the transitions during the rupture process of liquid bridges. The V regime transition was also found by Li and Sprittles [24] with low-Oh liquids, but the transition of the I regime in high-Oh liquids was not captured in Li's simulations. They provided an accurate phase diagram for the breakup of liquid bridges and identified the boundaries among different regimes.

E. Thermal fluctuations

More importantly, when $h_{\min}$ reduces to the molecular size, the dynamics of liquid bridges cannot be governed by the traditional Navier-Stokes equations under the continuity hypothesis [25–28]. The filament dynamics near pinch-off is mainly controlled by thermal fluctuations. However, due to the limitations of the temporal and spatial resolution in the experimental measurements, the effects of thermal fluctuations are hard to analyze at laboratory scale [29,30]. A powerful alternative is numerical methods, such as Lagrange particle-based molecular simulation (MD). MD gets rid of the boundary integral and interface tracking which are usually adopted in the Euler frame [31]. Moreover, the breakup dynamics can be well depicted in MD without using lubrication approximation and self-similar assumption in mathematical analysis for avoiding singularity in the equations. In particular, the effects of the thermal fluctuations can be investigated by MD, which is crucial in the rupture of microfluidics. Moseler and Landman first proposed a stochastic modification (SLE) instead of the deterministic lubrication equation (LE) to carry out the influences of the thermal fluctuations on jet breakup [32]. The analytical solutions were compared with the results of MD simulations, which suggest that the thermal fluctuations render liquid bridges form double-cone neck shapes near pinch-off. This new phenomenon cannot be captured by LE. The comparison of the growth rates in the liquid jets between MD outcomes and linear stability theory was presented by Choi *et al.* [33]. They revealed that the rupture time is obviously affected by the level of thermal fluctuations in the simulations. However, the high computational cost hinders the development of MD in investigating the dynamics of liquid bridges. In fact, the molecular details are relatively unimportant to pinch-off [34], so the coarse-grained method, as dissipative particle dynamics (DPD) [35–38], is a feasible avenue for studying the effects of the thermal fluctuations. The clogging of nanojets near the nozzle was first investigated by Tiwari and Abraham through DPD simulation [39]. They also summarized the relation between thermal length and rupture time with the frame of DPD [40]. The crossover problem between different regimes was discussed by Mo *et al.* [41,42]. They concluded that the crossover point is mainly dependent on the stochastic coefficient in DPD. The size of the thermal fluctuation dominated regime increases with the decreasing of the stochastic coefficient. However, the evaporation problem is non-negligible and its effect on the breakup of the liquid bridges is unknown in DPD [43]. This influence should be excluded in order to match with Rayleigh's assumption [26].

In the present study, we adopt many-body dissipative particle dynamics (MDPD), which is able to achieve the coexistence of vapor and liquid phases [44], to study the rupture dynamics and effects of the thermal fluctuations on the thinning of liquid bridges which we have used successfully in our previous work [45]. The aim of the present paper is to reveal the complete process of thinning liquid bridges including the I, V, VI, and thermal fluctuation (TF) regimes; reports of this are lacking in the previous literature. In addition, the transitions between different regimes are analyzed with various Oh numbers according to the variation of $h_{\min}$, maximum axial velocity $w_{\max}$, and $\mathrm{Re}_{\mathrm{local}}$, respectively. The effects of thermal fluctuations on the rupture dynamics of liquid bridges are focused on, especially for the formation of satellite drops with different Oh numbers.

Herein, we briefly revisit the background of MDPD, and give the relation between the MDPD simulation parameters and the real physical units in Sec. II. In addition the convergence of the present simulations is also discussed. Then the comparisons of growth rates between our results and the classical linear stability theory are provided in Sec. III. The complete process of liquid bridge thinning is analyzed and the transitions among different regimes are studied with the help of self-similar theory. Furthermore, the effects of the thermal fluctuations on the formation of satellite drops with different Oh numbers are investigated in detail. Finally, a brief conclusion is presented in Sec. IV.

II. SIMULATION METHODS

A. MDPD methods

MDPD is a method that deviates from the standard DPD to revise the quadratic relationship between pressure and density in the equation of state of DPD. The density-dependent conservative force $\boldsymbol{F}_{ij}^{C}$ is established to satisfy van der Waals equations for generating vapor and liquid coexistence, which is defined as

$$\boldsymbol{F}_{ij}^{C} = \left[A w^{C}(r_{ij}) + B(\overline{\rho_i} + \overline{\rho_j}) w_d^{C}(r_{ij})\right]\boldsymbol{e}_{ij}, \tag{5}$$

where the local densities $\overline{\rho_i}$ and $\overline{\rho_j}$ are accumulated by the weight function $w_\rho(r_{ij})$ as

$$w_\rho(r_{ij}) = \frac{15}{2\pi r_d^3}\left(1 - \frac{r_{ij}}{r_d}\right)^2, \tag{6}$$

where r_d is the cutoff radius for repulsive force. The coefficients A and B are used to describe the strength of attractive and repulsive forces, respectively.

Except for the conservative force, the forms of dissipative force $\boldsymbol{F}_{ij}^{D}$ and random force $\boldsymbol{F}_{ij}^{R}$ in MDPD are the same as those in the standard DPD as

$$\boldsymbol{F}_{ij}^{D} = -\gamma w^{D}(r_{ij})(\boldsymbol{v}_{ij}\cdot\boldsymbol{e}_{ij})\boldsymbol{e}_{ij}, \tag{7}$$

$$\boldsymbol{F}_{ij}^{R} = \xi w^{R}(r_{ij})\theta_{ij}\Delta t^{-1/2}\boldsymbol{e}_{ij}. \tag{8}$$

Herein, the dissipative parameter γ, random parameter ξ, and the corresponding weight functions should obey the fluctuation-dissipation theorem as

$$\gamma = \frac{\xi^2}{2k_B T}, \quad w^{D}(r_{ij}) = [w^{R}(r_{ij})]^2. \tag{9}$$

It is also introduced in the SLE [46]. Hence, the level of thermal fluctuations in MDPD is determined by the temperature T of the system. Δt is the interval of time in the simulations. All the particles in MDPD are governed by these three forces and follow Newton's second law.

The velocity-Verlet (VV) algorithm is widely adopted for integrating the MD and DPD systems because of its numerical stability and simplicity [47]. $\boldsymbol{F}_{ij}^{D}$ depends on the particle velocity and the force calculation contains a temporal misalignment between the position and velocity [48]. Hence, the modified velocity-Verlet (MVV) algorithm is used by Groot and Warren [37] and is expressed as

$$\begin{aligned}
\boldsymbol{r}_i(t+\Delta t) &= \boldsymbol{r}_i(t) + \Delta t\,\boldsymbol{v}_i(t) + \frac{1}{2m}(\Delta t)^2\boldsymbol{F}_i(t),\\
\boldsymbol{v}_i^{*}(t+\Delta t) &= \boldsymbol{v}_i(t) + \phi\Delta t\boldsymbol{F}_i(t),\\
\boldsymbol{F}_i(t+\Delta t) &= \boldsymbol{F}_i[\boldsymbol{r}(t+\Delta t), \boldsymbol{v}^{*}(t+\Delta t)],\\
\boldsymbol{v}_i(t+\Delta t) &= \boldsymbol{v}_i(t) + \frac{1}{2m}\Delta t[\boldsymbol{F}_i(t) + \boldsymbol{F}_i(t+\Delta t)].
\end{aligned} \tag{10}$$

In the MVV algorithm, the prediction of particle velocity $\boldsymbol{v}_i^{*}$ for the next step is first proposed before updating the real

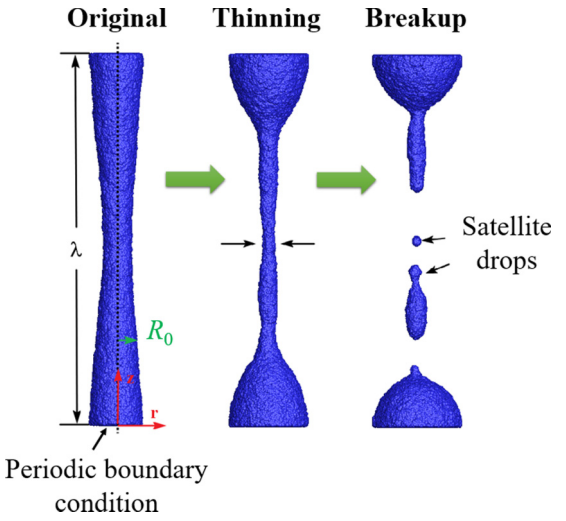

FIG. 1. Schematic of the rupture process of the liquid bridge. The periodic boundary condition is applied to mimic an infinitely long filament. The wavelength λ is managed to get different reduced wave number x. The liquid bridge gradually shrinks at the position of the minimum radius and pinches off to form satellite drops.

TABLE I. The liquid properties with different attractive coefficients A.

A	B	ρ	σ	μ	Oh	l_{v}	v_{c}	t_l	t_{v}
–50	25	6.9	13.01	7.22	0.311	0.581	1.802	10.703	0.322
–60	25	7.7	19.45	10.76	0.359	0.773	1.808	9.247	0.428
–70	25	8.4	26.76	18.31	0.499	1.499	1.461	8.215	1.026
–80	25	9.1	36.25	33.90	0.762	3.484	1.069	7.364	3.258
–90	25	9.8	47.30	64.01	1.214	8.836	0.739	6.690	11.956

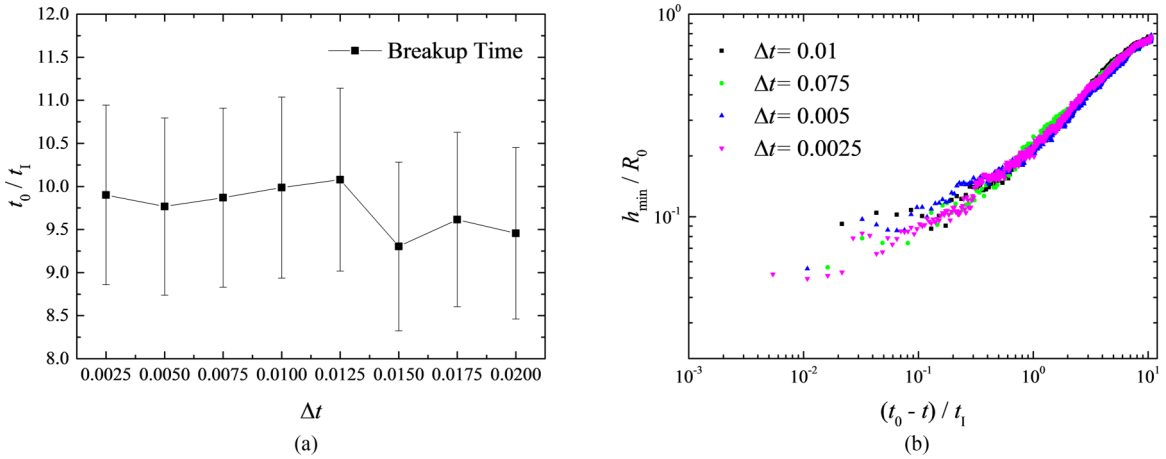

FIG. 2. (a) The variation of breakup time t_0 of liquid bridges with different Δt, ranging from 0.0025 to 0.02. The error bars show the standard deviation among the five repeated cases. (b) The variation of $h_{\min}$ with time under Δt from 0.01 to 0.0025.

velocity, and it is controlled by a factor ϕ. $\boldsymbol{v}^*$ is then used to calculate all kinds of force for the next step in MDPD, including $\boldsymbol{F}_{ij}^D$ which relies on particle velocity. The average of forces of current and the next step is used to reach the actual particle velocity $\boldsymbol{v}_i$. The MVV algorithm is suitable for MDPD without increase in computational cost. ϕ was tested in the standard DPD system by Groot and Warren and they found $\phi = 0.65$ is the optimal choice for the balance between system stability and computational efficiency. However, Zhang *et al.* proposed that $\phi = 0.55$ allows larger time steps in MDPD systems based on their numerical results [48]. In the present paper, we still adopt $\phi = 0.65$ for simulations as the temperature in our simulations can still be well controlled in this case. In addition, the random force is proportional to the inverse of the square root of Δt. Hence the specific choice of Δt might affect the strength of thermal fluctuation for liquid bridges. The detailed influences of Δt on the rupture of liquid bridges will be discussed in the next section.

B. Liquid bridges

There are three ways to investigate filament thinning: (1) Ejecting jets from nozzles with different velocities; (2) dipping droplets slowly under gravity; (3) unstabilizing liquid bridges with small perturbation. In the present study, we investigate the breakup process of an infinitely long liquid bridge. The self-similar solutions are only feasible when the slenderness assumption is valid [49,50]. The sinusoidal perturbation along the axis is imposed to make the liquid bridge unstable as

$$\frac{r(z)}{R_0} = 1 + \varepsilon \sin\left(x\frac{z}{R_0}\right), \tag{11}$$

where ε is the perturbation amplitude. x is the reduced wave number calculated by the wavelength λ:

$$x = \frac{2\pi R_0}{\lambda}. \tag{12}$$

The schematic diagram is shown in Fig. 1. λ is controlled to study different perturbations in order to compare the growth rates between simulations and theories.

The properties of liquids, such as density ρ, viscosity μ, and surface tension σ, can be controlled by the attractive A or repulsive B coefficients in conservative force as shown in Eq. (5). For simplicity, we adjust A to achieve different liquid properties with a fixed value of the repulsive parameter B in the present study. The viscosity is calculated by shear flow tests through the Lees-Edwards boundary condition as described in detail in our previous work [51]. The surface tension can be obtained by the fitting equation provided by Arienti *et al.* [52]:

$$\sigma^{fit} = -\frac{\pi}{240}\left(0.42Ar_c^5\rho^2 + 0.003Br_c^5\rho^3\right). \tag{13}$$

Furthermore, it is important to choose appropriate characteristic scales to normalize the physical units when carrying out scaling arguments and asymptotic analysis [53]. In the present simulations, the quantity of length was nondimen-

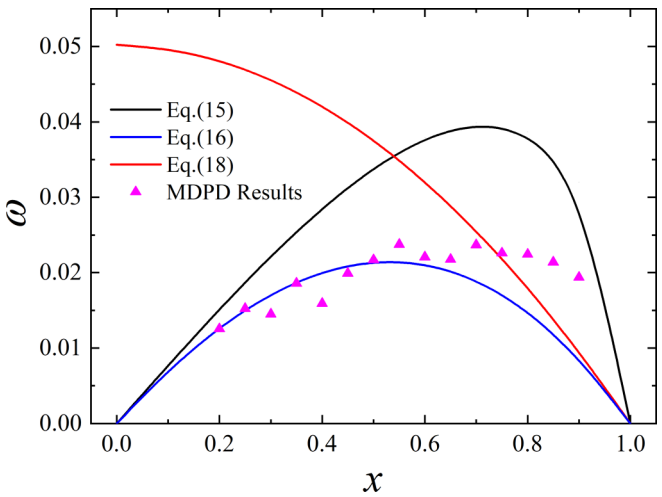

FIG. 3. The comparison of growth rate among MDPD results and three theories under Oh = 0.359. The sinusoidal perturbation is determined by the given x. According to Rayleigh instability, the liquid bridge begins to thin and break up eventually. For each value of x, the breakup time is monitored in order to get ω. The initial perturbations of $x = 0.2$ and 0.9 are also shown as snapshots.

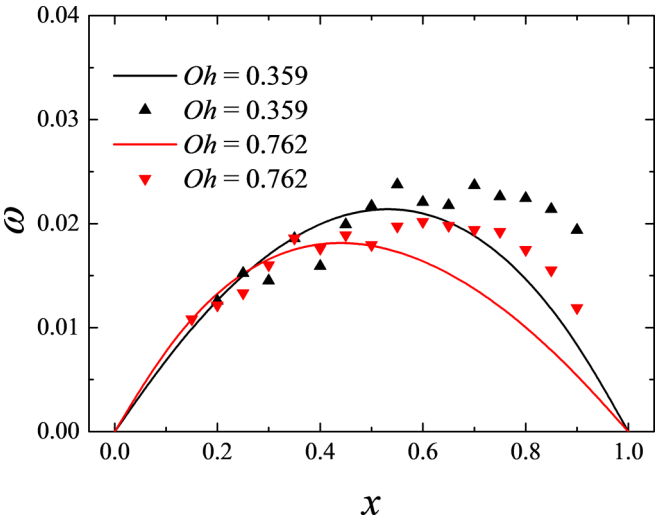

FIG. 4. Two Oh numbers are simulated to compare with Eq. (16). The black and red lines represent outcomes from Eq. (15) under the given Oh number. The discrete points are the growth rate obtained by MDPD simulations.

sionalized with the initial radius of the liquid bridge R_0. The intrinsic characteristic parameters of different fluids, such as viscous length scale l_v, viscous velocity v_c, and characteristic timescale t_I for low-Oh liquids and t_v for high-Oh liquids, are used to normalize the quantity of speed and time.

$$l_v = \frac{\mu^2}{\rho\sigma}, \quad v_c = \frac{\sigma}{\mu}, \quad t_I = \sqrt{\frac{\rho R_0^3}{\sigma}}, \quad t_v = \frac{\mu^3}{\rho\sigma^2}. \tag{14}$$

The values of these intrinsic characteristic parameters for different liquid properties are listed in Table I. The mapping between the MDPD parameters and real physical units is still ambiguous. The relation can be obtained through matching the dimensionless isothermal compressibility [54]. According to the dimensional analysis carried out by Arienti *et al.* [52], l_v and t_v for water are about 13.9 nm and 193 ps, respectively.

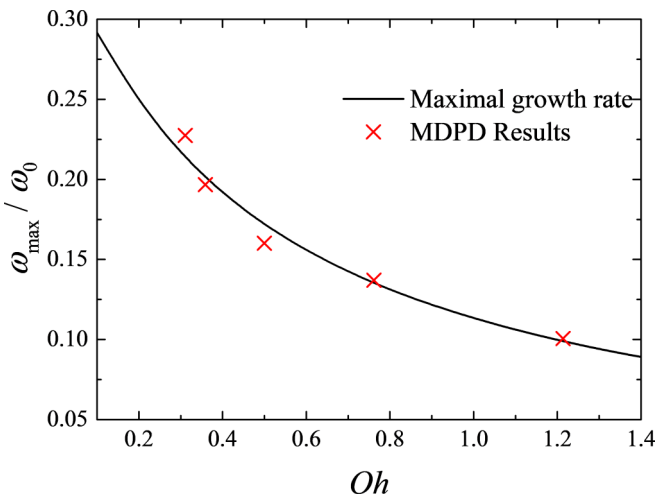

FIG. 5. The comparison of maximal growth rate ω_{max} between MDPD results and the analytical solution. ω_{max} is normalized by ω_0. The range of Oh numbers is from 0.311 to 1.214.

The length and time unit in MDPD can be calculated as $L_{MDPD} = 17.98$ nm and $T_{MDPD} = 450.93$ ps by matching the case of $A = -60$ with water where R_0 is equal to 6.0 in our simulation, suggesting that the radius of the liquid bridge is about 107.88 nm for real water.

III. RESULTS AND DISCUSSION

A. Thinning process of liquid bridges

First, we test the influence of Δt on the dynamics of liquid bridges. According to Groot and Warren's work, the stability of the system is kept if $\Delta t < 0.06$ under $\phi = 0.65$ in DPD. However, the critical Δt in MDPD should be smaller because of its nonlinear repulsive force. Therefore, we choose Δt ranging from 0.0025 to 0.02 to study its influence on the breakup time t_0 of a liquid bridge. The reduced wave number x is set as 0.3 and all the cases are repeated five times to obtain the average breakup time under different Δt. Figure 2(a) shows the variation of t_0 versus Δt. Based on Fig. 2(a), we find that t_0 is not obviously affected by Δt in our simulations. t_0 is ten times larger than t_I and remains stable when Δt is smaller than 0.0125. The occurrence of error bars is caused by the random fluctuations near rupture and the statistical errors in the simulations. Then we keep an eye on the detailed evolution of h_{min} under different Δt. Figure 2(b) suggests the variation of h_{min} with time. Although Δt will affect the strength of random force as shown in Eq. (8), it seems not to be evident to influence the dynamics of liquid bridges if Δt is less than 0.01, which is in agreement with the results of t_0. In summary, the influences of Δt on the dynamics of liquid bridges are relatively unimportant if Δt is small enough in the simulations. Hence, we set Δt as 0.01 in the following simulations to balance the computational accuracy and efficiency.

Next, we compare our results with linear stability theory. The perturbation on the profile of liquid bridges grows and

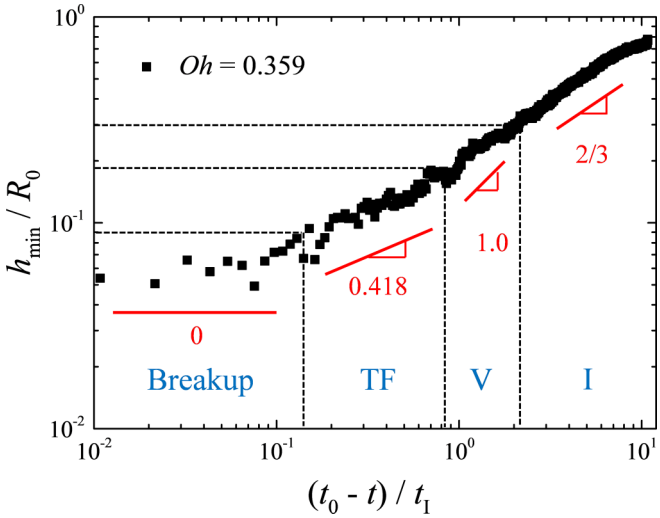

FIG. 6. The evolution of h_{min} with time under Oh = 0.359. The four regimes are observed according to scale fitting with self-similar theory. The TF regime is well described in the simulation and another regime, named the breakup regime, is captured.

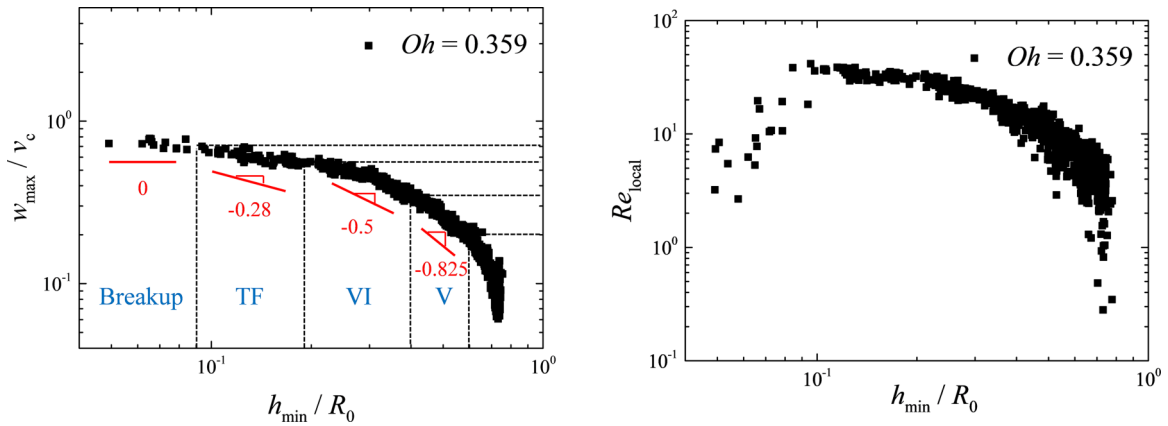

FIG. 7. (a) The variation of w_{max} with h_{min} for Oh $= 0.359$. The complete process is divided into four regimes where the transition from the V to the VI regime can be captured. (b) The variation of Re_{local} with h_{min}.

the surface area of the liquid bridge decreases. For inviscid incompressible liquids, this instability is caused by the competition between inertia and surface tension, and Rayleigh found the expression for growth rate ω, where effect of viscosity is ignored, as [8]

$$\omega = \omega_0 \sqrt{\frac{I_1(x)}{I_0(x)} x(1-x^2)}, \tag{15}$$

where $\omega_0 = 1/t_1$. $I_n(x)$ is the modified Bessel function of order n. ω is a real number with $x < 1$ and the perturbations will grow exponentially to make the jet unstable under any arbitrarily small perturbations. Inversely, the perturbations will be damped by viscosity eventually if $x > 1$. The maximum of ω for instability can be calculated according to Eq. (15), suggesting that the largest ω occurs when $x = 0.697$, which is the famous Rayleigh mode.

However, Eq. (15) is only valid for the assumption of inviscid and incompressible liquids and should be revised when the viscous effect becomes more and more important. Chandrasekhar [55] studied the effect of viscosity on instability through solving the Navier-Stokes equations and found

$$\omega = \omega_0 \left[\sqrt{\frac{1}{2}(x^2 - x^4) + \frac{9}{4}\mathrm{Oh}^2 x^4} - \frac{3}{2}\mathrm{Oh}x^2 \right]. \tag{16}$$

Here ω is a function of both x and the Oh number. The value of x for the fastest-growing mode is determined by the Oh number as

$$x = \sqrt{\frac{1}{2 + \sqrt{18}\mathrm{Oh}}}, \tag{17}$$

which decreases with large Oh number. As Oh increases continually, ω eventually only depends on the balance between surface tension and viscosity. Equation (17) changes into

$$\omega = \omega_v \tfrac{1}{6}(1 - x^2), \tag{18}$$

where $\omega_v = v_c/l_v = \sigma/\mu R_0$.

In our simulation, we achieve a wide range of ω by choosing x from 0.15 to 0.9. ω is measured by Cline and Anthony's experimental method [56], in which $\omega \sim 1/t_0$. Simulation results of Oh $= 0.359$ for growth rate compared with

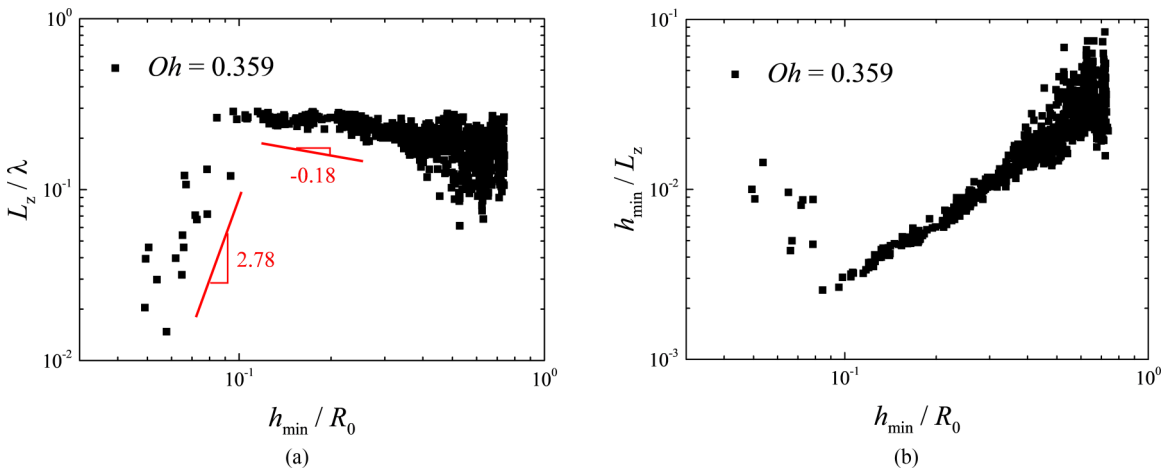

FIG. 8. (a) The evolution of L_z with h_{min} for Oh $= 0.359$. L_z first increases slowly in the period of thinning followed by $L_z \propto h_{min}^{-0.18}$, and then quickly reduces with the power law of $L_z \propto h_{min}^{2.78}$. (b) The variation of slenderness ratio h_{min}/L_z.

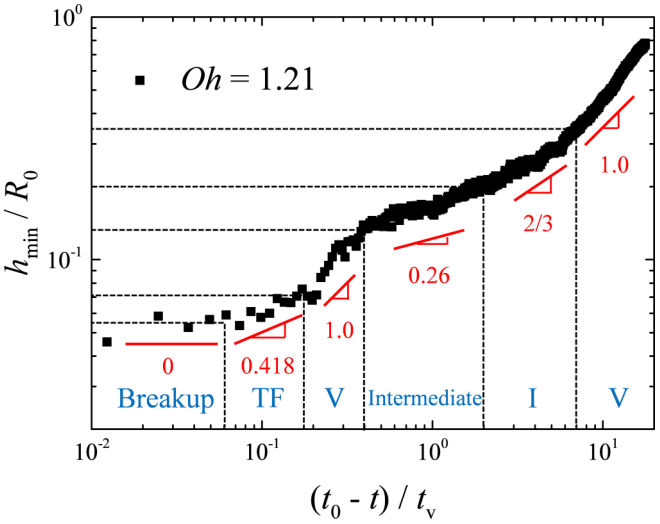

FIG. 9. The evolution of h_{min} with time to breakup under Oh = 1.21. The I regime is found in high-Oh liquids.

Eqs. (15), (16), and (18) are shown in Fig. 3. It suggests that our results fit well with Eq. (16) under small x. This indicates that the effects of surface tension and viscosity on ω are equally important for Oh = 0.359. However, the numerical results deviate from Eq. (16), but approach Eq. (15) with the increasing in x. This situation was also discovered in MD simulations [33], and it was believed that the dynamics of nanoscale liquid jets do not always follow the classical theories due to the existence of thermal fluctuations. Another possible reason for these deviations is that the Laplace pressure becomes higher with the increase of curvature under large x. Under this situation, the surface tension dominates the thinning process of the liquid bridges which makes the simulation results tend to Eq. (15). This deviation is also analyzed with different Oh numbers, as shown in Fig. 4. It indicates the comparison of ω between MDPD results and Eq. (16) for Oh = 0.359 and 0.762. A large Oh number, i.e., more viscous liquids, decreases ω and delays the time to breakup, but the deviation in Fig. 3 seems not to be recovered with a larger Oh number. Then we insert Eq. (17) into Eq. (16) to calculate the maximal growth rate ω_{max} with the range of Oh from 0.311 to 1.214. As shown in Fig. 5, the results from MDPD simulations are in good agreement with the prediction of the theory, which illustrates that the MDPD model can capture the thinning and rupture dynamics of liquid bridges. The specific advantage of MDPD is its ability to investigate the effects of thermal fluctuations.

Due to the unknown deviation under large x as discussed above, we choose $x = 0.3$ for the initial perturbation and change the Oh number to find out the transition in the period of liquid bridge thinning. The low-Oh liquids, i.e., Oh = 0.359, are studied first. According to the referenced plot (i.e., red lines) between h_{min} and time to breakup whose values are achieved by self-similar theory, the four regimes exiting in the period of liquid bridge thinning are observed. The detailed divisions are based on the points with minimal standard deviation between theoretical value and simulation results as shown in Fig. 6. First, h_{min} decreases along the 2/3 slope where surface tension dominates the thinning dynamics, and the numerical scaling number α of the best fitting in this region is about 0.634 calculated by the least-squares method. The I regime lasts until h_{min} decreases to about $0.26R_0$ and then the liquid bridge enters the V regime with theoretical $\alpha = 1.0$ and $\alpha = 0.973$ in the simulation. The V regime for low-Oh liquids is quite narrow, so Burton *et al.* thought that the I regime is enough to describe the breakup down to the nanoscale [57]. The V regime for low-Oh liquids was first revealed by Castrejón-Pita *et al.* [23] and then studied numerically by Li *et al.* [24] However, the transition from the V to the VI regime is hard to distinguish in Fig. 6, and evident division can be found with the aid of w_{max} and Re_{local}. Besides, with the transition from the I to the V regime, we can also get the TF regime when h_{min} reaches $0.17R_0$. The points distribute along the slope of 0.418, as obtained from the numerical solution for SLE [34], which is approximately equal to 0.396 in the case. In this region, the thermal fluctuations dominate the breakup dynamics of liquid bridges. In previous papers the TF regime is believed to be the final regime before rupture. Nevertheless in the present study, a new regime where α approaches zero is captured when h_{min} reaches $0.09R_0$. In this regime, h_{min}

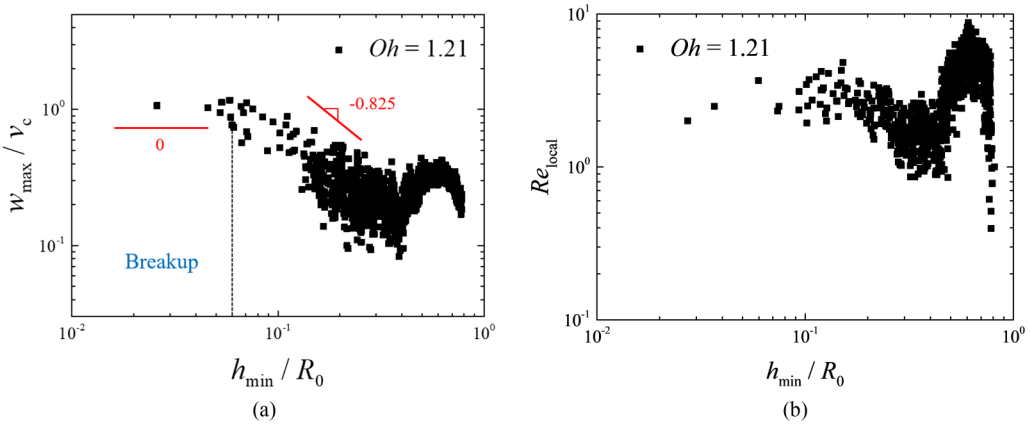

FIG. 10. (a) The variation of w_{max} with h_{min} for Oh = 1.21. (b) The variation of Re_{local} with h_{min}. The transition between different regimes can be captured depending on the value of Re_{local}.

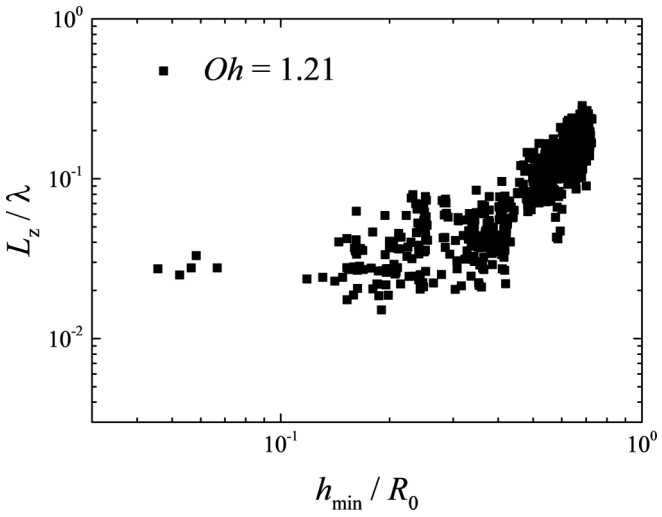

FIG. 11. The evolution of L_z with h_{min} for Oh = 1.21. The increase near pinch-off captured in the fluid of Oh = 0.359 cannot be found here in the high-Oh situation.

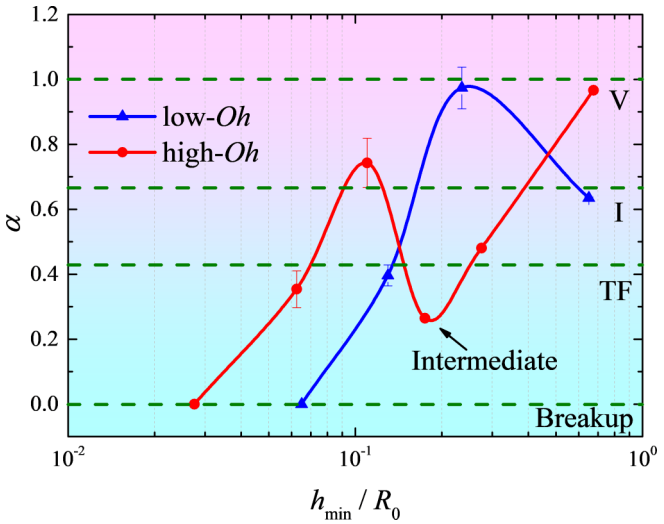

FIG. 12. The trajectory of α for low-Oh (blue line) and high-Oh (red line) liquids during thinning. The points without error bars mean that the error bar is smaller than the point.

remains relatively constant regardless of the time. We name this regime as the breakup regime where self-similar theory seems to be invalid.

Then we focus on the evolution of w_{max} to clarify the transition between different regimes. The relation between w_{max} and h_{min} in the V and VI regimes is given by [18–20]

$$w_{max} \propto h_{min}^{-0.5}(\mathrm{V}), \quad w_{max} \propto h_{min}^{-0.875}(\mathrm{VI}). \tag{19}$$

Figure 7(a) shows that w_{max} increases with the thinning of the liquid bridge. Based on the referenced slope line, the transition from the V to the VI regime can be roughly determined through the magnitude of α, and it is consistent with previous work [23,24]. It is interesting to note that the V regime determined by w_{max} is larger than that according to h_{min}, which suggests that the clear division from the I to the V regime during thinning of the liquid bridges is still hard to achieve. However, the boundary between the TF and V regimes is basically identical whichever variables we observe. Additionally, α for w_{max} in the TF regime is about –0.28 and drops to 0 in the breakup regime. In the breakup regime, w_{max} stays constant and is the same order of intrinsic viscous velocity of the liquid with Oh = 0.359.

Then we further investigate the dynamic of liquid bridges by analyzing Re_{local} along liquid bridges. Re_{local} is defined as

$$\mathrm{Re}_{local} = \frac{\rho L_z w_z}{\mu}. \tag{20}$$

Here L_z is the distance along the axial direction between the local point and the pinch point h_{min}, and w_z is the axial velocity of the local point. However, the definition of local point is not unique. In Castrejón-Pita's work, they chose the position where its radius is $1.2h_{min}$ as the local point [23], but this definition is ambiguous in physics. Therefore, we adopt the definition provided in Li's paper where the local point is the position of maximum axial velocity w_{max}. So $L_z = |z(r = h_{min}) - z(w_z = w_{max})|$ and $w_z = w_{max}$ in Eq. (20). Figure 7(b) shows that Re_{local} increases in the thinning process, like the performance of w_{max}, but it drops rapidly to $\mathcal{O}(10^0)$ when h_{min} is smaller than $0.1R_0$, which suggests that the liquid bridge enters the TF and breakup regimes. However, the obvious transition from the I to the V regime is difficult to capture in Fig. 7. According to the definition of Re_{local} in Eq. (20), Re_{local} is proportional to L_z and w_{max}. w_{max} remains stable near breakup, which suggests that L_z is obviously changed when the liquid bridge reaches rupture. Figure 8(a) indicates the exponent relation between L_z and h_{min}. During the thinning process of the liquid bridge, L_z gradually increases, suggesting that the point of w_{max} goes far away from the pinch point. However, the position of w_{max} is rapidly close to the pinch point when the liquid bridge starts to pinch off. The exponent relation is obtained from the simulations as

$$L_z \propto h_{min}^{-0.18}(\mathrm{thinning}), \quad L_z \propto h_{min}^{2.78}(\mathrm{breakup}). \tag{21}$$

L_z is believed to play a crucial role in the formation of satellite drops [49,58]. Then the slenderness ratio h_{min}/L_z is demonstrated in Fig. 8(b). h_{min}/L_z decreases to $\mathcal{O}(10^{-3})$ before the liquid bridge begins to break up, and it makes the assumption of a long slender bridge in self-similar theory valid. In this region, lubrication approximation works well to describe the dynamics of liquid bridges. However, the validation of this assumption is questionable since h_{min}/L_z increases near the pinch-off time. Hence, more detailed studies about the rupture dynamics of liquid bridges need to be done.

Then we focus on the transition in the period of thinning for high-Oh liquids, i.e., Oh = 1.21. The variation of h_{min} with time is shown in Fig. 9. The liquid bridge starts to thin in regime V because the l_v of Oh = 1.21 is larger than the observation scale of R_0, where α is 0.967. Then it enters into regime I (i.e., $\alpha = 0.48$). Before the liquid bridge reenters the V and VI regimes until h_{min} reduces to $0.06R_0$, it experiences an intermediate regime (i.e., $\alpha = 0.26$) which cannot be found in self-similar theory but really exists according to experiments [23]. The TF and breakup regimes are also observed

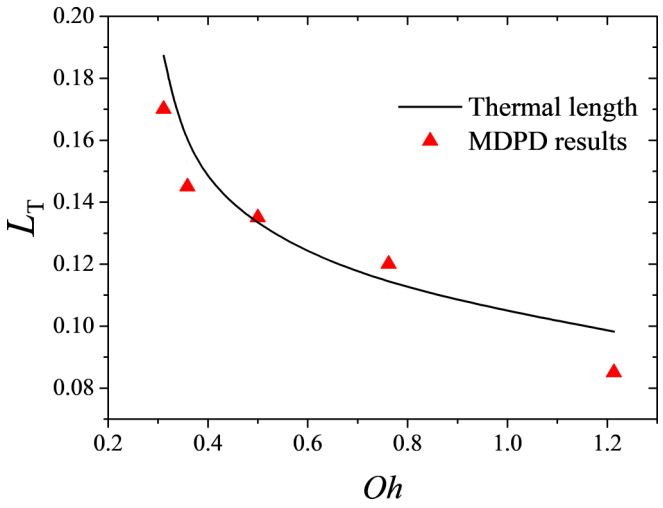

FIG. 13. The comparison between crossovers from the VI to the TF regime and thermal length L_T under different Oh numbers.

when the filament approaches pinch-off. The presence of the I regime in high-Oh liquids is discussed by Castrejón-Pita [23]. They pointed out that the rupture process of high-Oh liquids consists of many intermediate regimes, and the transitions are more complicated compared with low-Oh liquids. The w_{max} and Re_{local} are indicated in Fig. 10. w_{max} increases with the power law $\alpha = 0.825$, implying that it locates in the V regime. It becomes stable and equals v_c near pinch-off, which is similar with the tendency in low-Oh liquids. Referring to the value of Re_{local}, the transitions of different regimes can be identified more clearly. Re_{local} is $\mathcal{O}(10^0)$ first and increases to $\mathcal{O}(10^1)$ where the effect of inertia increasingly becomes dominant. Then it drops down to $\mathcal{O}(10^0)$ again. In the end, Re_{local} increases slowly, showing the transition from the V to the VI regime. It is not able to divide the VI regime and the TF regime according to Re_{local}. The existence of regime I is believed to be one of the reasons for forming a visible satellite drop even in a high-Oh liquid. L_z is also monitored in Fig. 11. L_z decreases monotonously during thinning and then remains stable near breakup, which is quite different from low-Oh liquids. The detailed analysis of this phenomenon will be discussed in the next section based on the effects of thermal fluctuations on the formation of satellite drops.

Finally, the complete processes for low- and high-Oh liquid bridges are listed in Fig. 12. For low-Oh liquid bridges, the trajectory of α is relatively simple. It starts near the I regime and approaches the V regime following with the decrease in h_{min}. Then α rapidly reduces if the liquid bridges reach pinch-off. It is important to note that the TF regime is not the final regime before pinch-off. α will continue to decrease to zero until the breakup of the liquid bridges, so the whole process of low-Oh liquid bridges is I → V → VI → TF → breakup. Relatively, the liquid bridges with high Oh show more complex behaviors. The main difference compared with low-Oh liquid bridges is that high-Oh liquid bridges begin near the V regime and subsequently enter the I regime and an unexplored intermediate regime. After that it returns to the V regime and the residual process is similar to that of low-Oh liquid bridges. Therefore, V → I → Intermediate V → VI → TF breakup is the complete process for high-Oh liquid bridges. Although the liquid bridges for low and high Oh both experience the TF and breakup regimes before rupture, the detailed dynamics of breakup under different Oh numbers are not the same, which will be studied by considering the effects of thermal fluctuations.

B. Effects of thermal fluctuations on satellite drops

One of the most common phenomena during the breakup of liquid bridges is the appearance of satellite drops. Satellite drops are undesirable in printing technology since it will decrease the fidelity of the final results. For electronic devices in nanoscale, it will lead to broken or short circuits, making the device fail. Hence, the understanding of the drop-formation process is considerably important to manage and eliminate satellite drops. As the formation of satellite drops is significantly affected by the states of liquid bridges closing to breakup, at the same time, the breakup dynamics are dominated by thermal fluctuations, so it is reasonable to deduce that thermal fluctuations play a crucial role in satellite drops [22,57,59]. In order to investigate the influence of thermal fluctuations, we use a thermal length scale L_T to express the strength of thermal fluctuations in the present

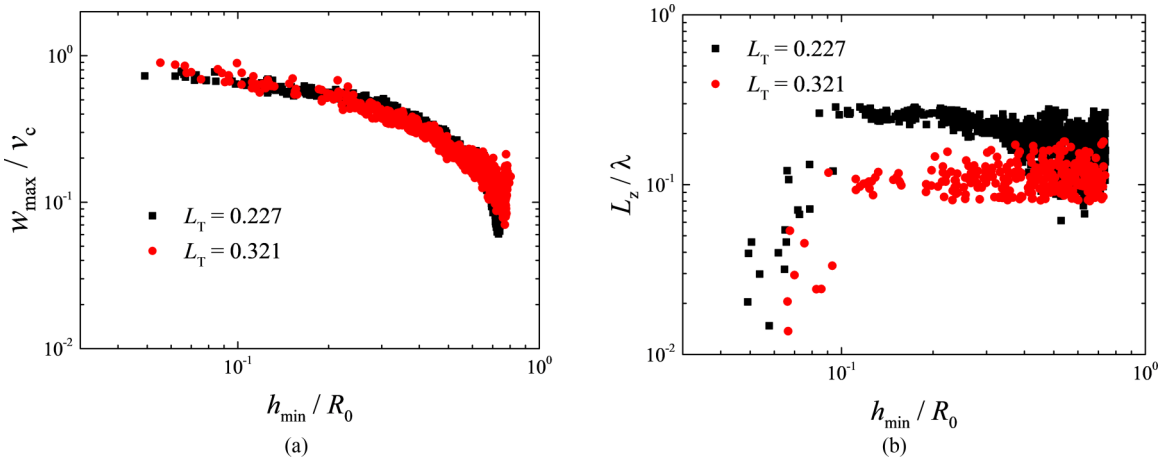

FIG. 14. The comparison between $L_T = 0.227$ and 0.321 under Oh = 0.359. (a) w_{max}; (b) L_z.

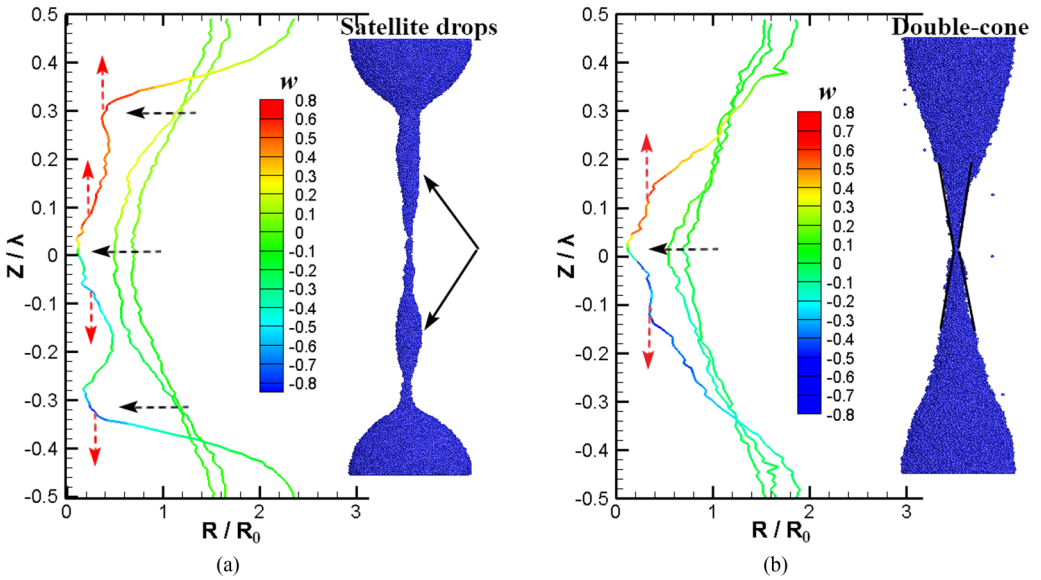

FIG. 15. The axial velocity w along the axis with different L_T and the snapshot near pinch-off. (a) $L_T = 0.227$. (b) $L_T = 0.321$. Three positions of the liquid bridge thin simultaneously to form satellite drops with weak thermal fluctuations. Only one position thins with strong thermal fluctuations to generate a double-cone shape without satellite drops.

simulations as [40]

$$L_T = \sqrt{\frac{k_B T}{\sigma}}, \tag{22}$$

where k_B is the Boltzmann constant and T is the temperature of the system. If L_T is large enough, i.e., $h_{min} < L_T$, thermal fluctuations will dominate the thinning process of the liquid bridges. According to Eq. (22), the value of L_T is determined by T and σ. In the present work, we only vary T to control the strength of thermal fluctuations rather than changing the surface tension of the liquid bridges. In addition, the dissipative parameter γ in Eq. (7) is kept constant in order to keep the same viscous effect during the thinning process. The transition from the VI to the TF regime is affected by L_T as shown in Fig. 13. The red scatters indicate the crossovers from the VI to the TF regime in the simulations and the black line shows L_T calculated by Eq. (22). We find that the crossovers are proportional to L_T and transition happens when h_{min} is smaller than L_T, which is in agreement with the previous experimental work [59]. Small L_T will delay the transition and decrease the size of the TF regime. Additionally, the TF regime is supposed to have evident repercussions on the formation of satellite drops [59].

Then we study the effects of the thermal fluctuations on satellite drops under different Oh numbers, especially for the time closing to rupture. First, the low-Oh liquids, i.e., Oh = 0.359, are selected to investigate the variation of L_z and axial velocity w with different L_T. The comparisons of L_z and w_{max} between different L_T during thinning in low-Oh liquids are showed in Fig. 14. w_{max} is not obviously affected by L_T as shown in Fig. 14(a). However, the strong thermal fluctuations reduce the distance between the pinching point and the maximal axial velocity during thinning. This situation is caused by the different distributions of w along the axial direction and determines the shapes of the liquid bridges near pinch-off. Figure 15 shows the distribution of w along the axial direction with different L_T and the snapshots of the liquid bridges close to breakup. Under weak thermal fluctuations, there are three points thinning simultaneously because of the multipeaks of w along the liquid filament in Fig. 15(a). Satellite drops form between the peaks of w. However, the strong thermal fluctuations smooth the distribution of w and only one position of the liquid bridge thins as shown in Fig. 15(b). In this condition, the double-cone apex is captured, which has been discovered in MD simulations [32]. Liquids retract to either side and do not form satellite drops. The comparison of w between different thermal fluctuations when the liquid bridge approaches to breakup is indicated in Fig. 16. Four peaks are found when the thermal fluctuations are weak, while there are only two peaks when the thermal

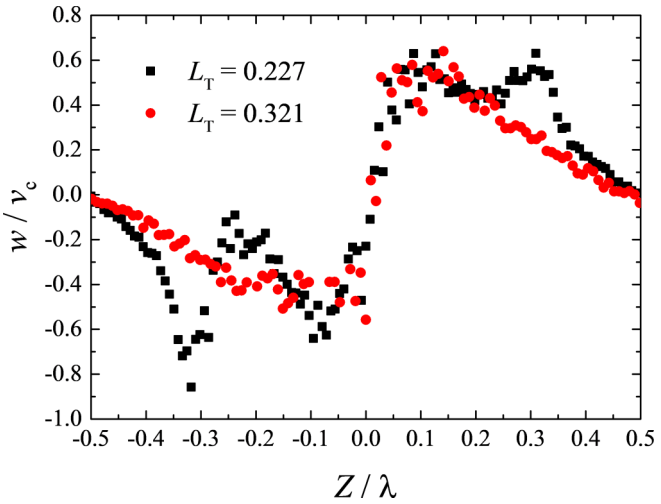

FIG. 16. The comparison of w along the axial direction between different L_T when the liquid bridge approaches breakup under Oh = 0.359.

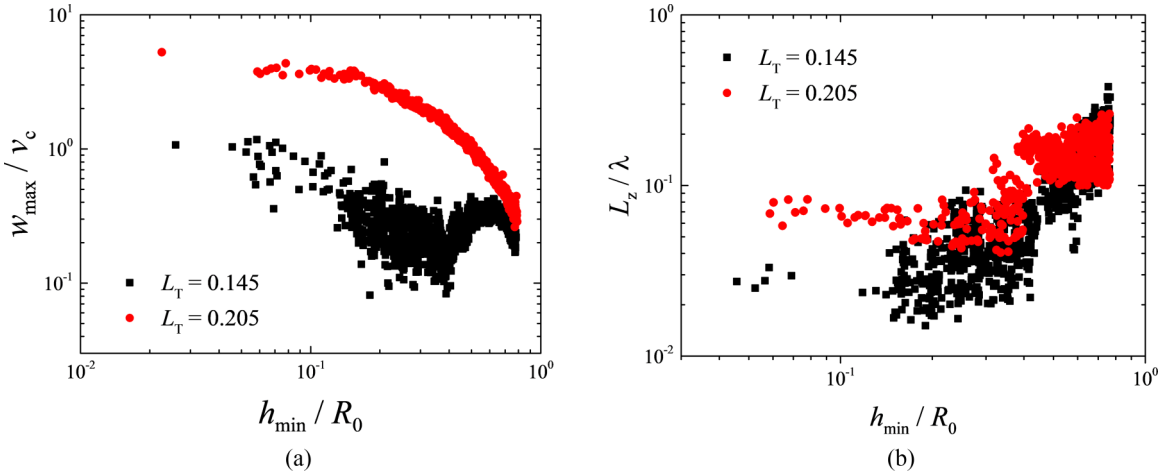

FIG. 17. The comparison between $L_T = 0.145$ and 0.205 under Oh = 1.21. (a) w_{max}; (b) L_z.

fluctuations become stronger. w_{max} and the positions of the peaks seem not to be affected by L_T. It suggests that the stronger thermal fluctuations in low-Oh liquids smooth the distribution of w and reduce the distance between velocity peaks which is the key for eliminating the formation of satellite drops. Nevertheless, the situation is totally different for liquid bridges with high-Oh number, i.e., Oh = 1.21. The liquid bridge becomes tenuous if the viscosity increases and the breakup point seems to locate at a random point [9,31]. Figure 17 expresses the comparison of L_z and w_{max} between different L_T under large Oh. w_{max} now obviously increases under strong thermal fluctuations in high-Oh liquids as shown in Fig. 17(a), and L_z also extends, which is inverse to the situation in the low-Oh liquids. Thus the effects of the thermal fluctuations on the formation of satellite drops are totally different for low- and high-Oh liquids. To investigate this influence in detail, the distribution of w along the axial direction and the snapshots near pinch-off are provided in Fig. 18. Figure 18(a) shows that the pinch point stays in the middle of the liquid bridge and the distance of the peaks of w is relatively short without formation of satellite drops, but this distance becomes long if the thermal fluctuations are stronger. The liquid filament breaks up on both ends and generates a large satellite drop in the middle, as shown in Fig. 18(b). According to the distribution of w near pinch-off in Fig. 19, the value w_{max} is significantly increased by strong thermal fluctuations. A wide region with small w exists and the pinch points depart away from each one to generate a large satellite drop. In Castrejón-Pita's conclusion, they deduced that the presence of the intermediate I regime is the reason for forming visible satellite drops even in the breakup of high viscous liquids [23]. However, the simulation in the present study

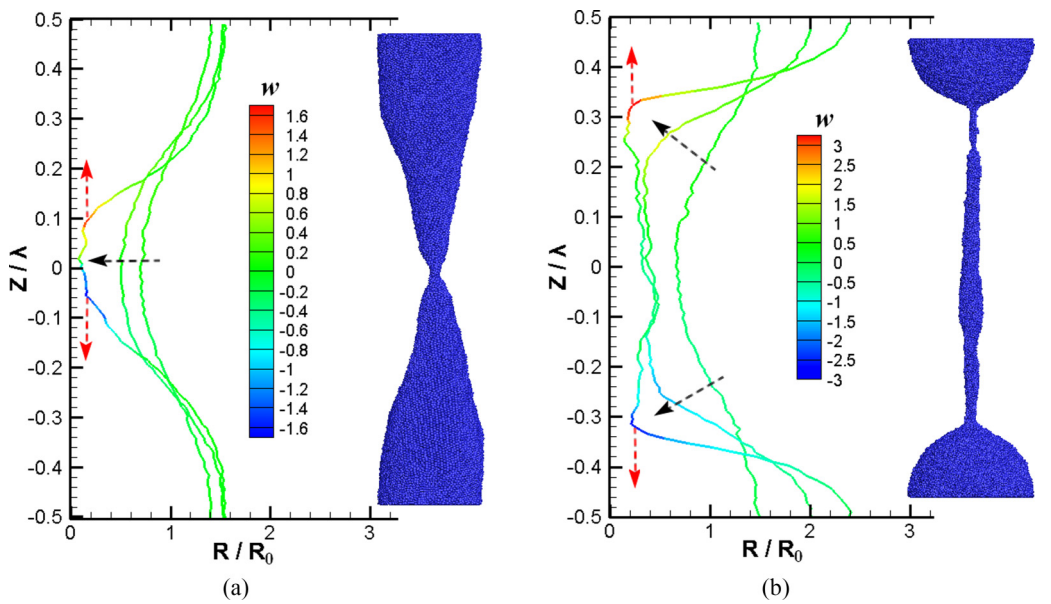

FIG. 18. The axial velocity w along the axis with different L_T and the snapshot near pinch-off. (a) $L_T = 0.145$. (b) $L_T = 0.205$. The strong thermal fluctuations increase the distance between peaks of w and form a large satellite drop in the middle.

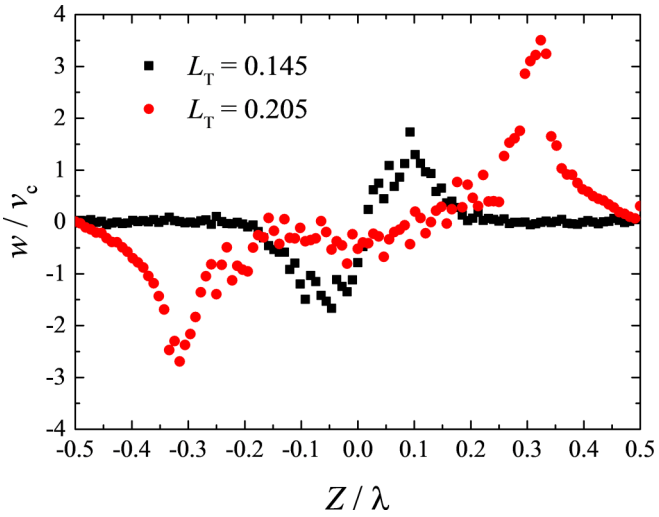

FIG. 19. The comparison of w along the axial direction between different L_T when the liquid bridge approaches breakup under Oh = 1.21.

demonstrates that the formation of the satellite drops may be mainly influenced by the thermal fluctuations on the position of the peaks of axial velocity.

In summary, for low-Oh liquids the thermal fluctuations tend to smooth the distribution of the axial velocity to eliminate the multipeaks without changing its maximal value, and it results in the appearance of the double-cone apex. Contrarily, the distance between the peaks of axial velocity is greatly extended by the thermal fluctuations in high-Oh liquids to form a wide range of small axial velocity, which generates a large satellite drop in the middle.

IV. CONCLUSION

The complete thinning processes of liquid bridges are investigated by the particle-based method known as many-body dissipative particle dynamics (MDPD). The growth rates of the liquid bridges are compared with the linear stability theory with different Ohnesorge numbers (Oh). The deviations from the theoretical results in the simulations under large wave number x are studied. Larger curvature in the profile of the liquid bridge under large x is one of the reasons for this difference, as also discussed in molecular simulations (MD). The transitions during thinning among inertial (I), viscous (V), viscous-inertial (VI), and thermal fluctuations (TF) are analyzed depending on the scaling numbers α in minimal radius h_{min}, maximal axial velocity w_{max}, and local Reynolds number Re_{local} which are calculated by the classical self-similar theory. It is worth noting that another regime called the breakup regime is described in the present work. In the breakup regime, h_{min} basically remains constant until rupture and the distance L_z along the axial direction between the point of w_{max} and the pinch point h_{min} decreases evidently in low-Oh liquids and remains stable in high-Oh liquids. The whole trajectories of thinning liquid bridges are I $\rightarrow$ V $\rightarrow$ VI $\rightarrow$ TF $\rightarrow$ breakup for low-Oh liquids and V $\rightarrow$ I $\rightarrow$ Intermediate $\rightarrow$ V $\rightarrow$ VI $\rightarrow$ TF $\rightarrow$ breakup for high-Oh liquids, respectively.

Furthermore, the effects of the thermal fluctuations on the formation of satellite drops are studied for low-Oh and high-Oh liquids. Strong thermal fluctuations cause the liquid bridge shape to change into a double cone and eliminate the satellite drops. The distribution of axial velocity is smoothed by strong thermal fluctuations compared with the situation under weak thermal fluctuations where multipeaks are found to result in multiple satellite drops. The role of the thermal fluctuations in high-Oh liquids is quite different. The distance between peaks of axial velocity is extended by strong thermal fluctuations to form a wide region of small axial velocity. The liquid filament breaks up on both ends and forms a large satellite drop. Therefore, the thermal fluctuations may be the key reason for the formation of satellite drops in the rupture of high viscous liquids. This research is of help in understanding the mechanism of the formation of satellite droplets and provides a potential method to manage the satellite droplets when liquid bridges break up.

ACKNOWLEDGMENTS

This work was supported by the National Natural Science Foundation of China (Grants No. 11872283 and No. 11902188) and Shanghai Sailing Program (Grant No. 20YF1432800). The grants are gratefully acknowledged.

[1] H. T. Chen, A. J. Taylor, and N. Yu, A review of metasurfaces: Physics and applications, Rep. Prog. Phys. **79**, 076401 (2016).
[2] O. A. Basaran, H. Gao, and P. P. Bhat, Nonstandard inkjets, Annu. Rev. Fluid Mech. **45**, 85 (2013).
[3] Y. Y. Ye, R. Biswas, J. R. Morris, A. Bastawros, and A. Chandra, Molecular dynamics simulation of nanoscale machining of copper, Nanotechnology **14**, 390 (2003).
[4] M. J. Heller, DNA microarray technology: Devices, systems, and applications, Annu. Rev. Biomed. Eng. **4**, 129 (2002).
[5] P. Calvert, Materials science. Printing cells, Science **318**, 208 (2007).
[6] H. A. Stone, A. D. Stroock, and A. Adjari, Engineering flows in small devices: Microfluidics toward a lab-on-a-chip, Annu. Rev. Fluid Mech. **36**, 381 (2004).
[7] J. Plateau, Experimental and theoretical researches on the figures of equilibrium of a liquid mass withdrawn from the action of gravity. Third series, Philos. Mag., Ser. 4 **14**, 431 (1857).
[8] L. Rayleigh, On the instability of jets, Proc. London Math. Soc. **s1-10**, 4 (1878).
[9] J. Eggers, Nonlinear dynamics and breakup of free-surface flows, Rev. Mod. Phys. **69**, 865 (1997).
[10] O. Reynolds, On the theory of lubrication and its application to Mr. Beauchamp tower's experiments, including an experimental determination of the viscosity of olive oil, Philos. Trans. R. Soc. London **177**, 157 (1886).
[11] M. P. Brenner, J. R. Lister, and H. A. Stone, Pinching threads, singularities and the number 0.0304 …, Phys. Fluids **8**, 2827 (1996).

[12] A. U. Chen and O. A. Basaran, A new method for significantly reducing drop radius without reducing nozzle radius in drop-on-demand drop production, Phys. Fluids **14**, L1 (2002).
[13] R. M. S. M. Schulkes, The evolution and bifurcation of a pendant drop, J. Fluid Mech. **278**, 83 (1994).
[14] J. B. Keller and M. J. Miksis, Surface tension driven flows, SIAM J. Appl. Math. **43**, 268 (1983).
[15] Y. J. Chen and P. H. Steen, Dynamics of inviscid capillary breakup: Collapse and pinchoff of a film bridge, J. Fluid Mech. **341**, 245 (1997).
[16] R. F. Day, E. J. Hinch, and J. R Lister, Self-Similar Capillary Pinchoff of an Inviscid Fluid, Phys. Rev. Lett. **80**, 704 (1998).
[17] W. Du, T. Fu, C. Zhu, Y. Ma, and H. Z. Li, Breakup dynamics for high-viscosity droplet formation in a flow-focusing device: Symmetrical and asymmetrical ruptures, AIChE J. **62**, 325 (2016).
[18] D. T. Papageorgiou, On the breakup of viscous liquid threads, Phys. Fluids **7**, 1529 (1995).
[19] G. H. Mckinley and A. Tripathi, How to extract the Newtonian viscosity from capillary breakup measurements in a filament rheometer, J. Rheol. **44**, 653 (2000).
[20] J. Eggers, Universal Pinching of 3D Axisymmetric Free-Surface Flow, Phys. Rev. Lett. **71**, 3458 (1993).
[21] O. A. Basaran, Small-scale free surface flows with breakup: Drop formation and emerging applications, AIChE J. **48**, 1842 (2002).
[22] J. Eggers, Drop formation—an overview, Z. Angew. Math. Mech. **85**, 400 (2005).
[23] J. R. Castrejón-Pita, A. A. Castrejón-Pita, S. S. Thete, K. Sambath, I. M. Hutchings, J. Hinch, J. R. Lister, and O. A. Basaran, Plethora of transitions during breakup of liquid filaments, Proc. Natl. Acad. Sci. USA **112**, 4582 (2015).
[24] Y. Li and J. E. Sprittles, Capillary breakup of a liquid bridge: Identifying regimes and transitions, J. Fluid Mech. **797**, 29 (2016).
[25] S. Kawano, Molecular dynamics of rupture phenomena in a liquid thread, Phys. Rev. E **58**, 4468 (1998).
[26] H. Shin, M. Oschwald, M. M Micci, and W. Yoon, Influence of thermodynamic state on nanojet break-up, Nanotechnology **16**, 2838 (2005).
[27] H.-h. Shin, D. Suh, and W.-s. Yoon, Non-equilibrium molecular dynamics of nanojet injection in a high pressure environment, Microfluid. Nanofluid. **5**, 561 (2008).
[28] W. Kang and U. Landman, Universality Crossover of the Pinch-Off Shape Profiles of Collapsing Liquid Nanobridges in Vacuum and Gaseous Environments, Phys. Rev. Lett. **98**, 064504 (2007).
[29] P. Zhu, X. Tang, Y. Tian, and L. Wang, Pinch-off of microfluidic droplets with oscillatory velocity of inner phase flow, Sci. Rep. **6**, 31436 (2016).
[30] A. U. Chen, P. K. Notz, and O. A. Basaran, Computational and Experimental Analysis of Pinch-Off and Scaling, Phys. Rev. Lett. **88**, 174501 (2002).
[31] J. Eggers and E. Villermaux, Physics of liquid jets, Rep. Prog. Phys. **71**, 036601 (2008).
[32] M. Moseler and U. Landman, Formation, stability, and breakup of nanojets, Science **289**, 1165 (2000).
[33] Y. S. Choi, S. J. Kim, and M. Kim, Molecular dynamics of unstable motions and capillary instability in liquid nanojets, Phys. Rev. E **73**, 016309 (2006).
[34] J. Eggers, Dynamics of liquid nanojets, Phys. Rev. Lett. **89**, 084502 (2002).
[35] P. J. Hoogerbrugge and J. M. V. A. Koelman, Simulating microscopic hydrodynamic phenomena with dissipative particle dynamics, Europhys. Lett. **19**, 155 (1992).
[36] P. Español, Hydrodynamics from dissipative particle dynamics, Phys. Rev. E **52**, 1734 (1995).
[37] R. D. Groot and P. B. Warren, Dissipative particle dynamics: Bridging the gap between atomistic and mesoscopic simulation, J. Chem. Phys. **107**, 4423 (1997).
[38] P. Español and P. B. Warren, Statistical mechanics of dissipative particle dynamics, Europhys. Lett. **30**, 191 (1995).
[39] A. Tiwari and J. Abraham, Dissipative particle dynamics simulations of liquid nanojet breakup, Microfluidics Nanofluidics **4**, 227 (2008).
[40] A. Tiwari, H. Reddy, S. Mukhopadhyay, and J. Abraham, Simulations of liquid nanocylinder breakup with dissipative particle dynamics, Phys. Rev. E **78**, 016305 (2008).
[41] C. Mo, L. Yang, F. Zhao, and K. Cui, Mesoscopic simulation of a thinning liquid bridge using the dissipative particle dynamics method, Phys. Rev. E **92**, 023008 (2015).
[42] C.-j. Mo, L.-z. Qin, and L.-j. Yang, Crossover behaviour study of a thinning liquid bridge using the dissipative particle dynamics method, Comput. Fluids **157**, 232 (2017).
[43] J. R. Lister and H. A. Stone, Capillary breakup of a viscous thread surrounded by another viscous fluid, Phys. Fluids **10**, 2758 (1998).
[44] P. B. Warren, Vapor-liquid coexistence in many-body dissipative particle dynamics, Phys. Rev. E **68**, 066702 (2003).
[45] J. Zhao, N. Zhou, K. Zhang, S. Chen, and Y. Liu, Study on stretching liquid bridges with symmetric and asymmetric surface wettability, Phys. Rev. Fluids **5**, 064003 (2020).
[46] R. F. Fox and G. Uhlenbeck, Contributions to non-equilibrium thermodynamics. I. Theory of hydrodynamic fluctuations, Phys. Fluids **13**, 1893 (1970).
[47] M. Allen and D. Tildesley, *Computer Simulation of Liquids*, 2nd ed. (Oxford University Press, Oxford, 2017).
[48] K. Zhang, Z. Li, M. Maxey, S. Chen, and G. E. Karniadakis, Self-cleaning of hydrophobic rough surfaces by coalescence-induced wetting transition, Langmuir **35**, 2431 (2019).
[49] L. Campo-Deaño and C. Clasen, The slow retraction method (SRM) for the determination of ultra-short relaxation times in capillary breakup extensional rheometry experiments, J. Non-Newtonian Fluid Mech. **165**, 1688 (2010).
[50] W. Mathues, C. McIlroy, O. G. Harlen, and C. Clasen, Capillary breakup of suspensions near pinch-off, Phys. Fluids **27**, 093301 (2015).
[51] J. Zhao, S. Chen, and N. Phan-Thien, Viscometric flow for a many-body dissipative particle dynamics (MDPD) fluid with Lees-Edwards boundary condition, Mol. Simul. **44**, 213 (2018).
[52] M. Arienti, W. Pan, X. Li, and G. Karniadakis, Many-body dissipative particle dynamics simulation of liquid/vapor and liquid/solid interactions, J. Chem. Phys. **134**, 204114 (2011).
[53] O. E. Yildirim and O. A. Basaran, Deformation and breakup of stretching bridges of Newtonian and shear-thinning liquids:

Comparison of one- and two-dimensional models, Chem. Eng. Sci. **56**, 211 (2001).

[54] Q. Nie, Y. Zhong, and H. Fang, Study of a nanodroplet breakup through many-body dissipative particle dynamics, Phys. Fluids **31**, 042007 (2019).

[55] S. Chandrasekhar, *Hydrodynamic and Hydromagnetic Stability* (Oxford University Press, Oxford, 1961).

[56] H. E. Cline and T. R. Anthony, The effect of harmonics on the capillary instability of liquid jets, J. Appl. Phys. **49**, 3203 (1978).

[57] J. C. Burton, J. E. Rutledge, and P. Taborek, Fluid Pinch-Off Dynamics at Nanometer Length Scales, Phys. Rev. Lett. **92**, 244505 (2004).

[58] P. P. Bhat, S. Appathurai, M. T. Harris, M. Pasquali, G. H. McKinley, and O. A. Basaran, Formation of beads-on-a-string structures during break-up of viscoelastic filaments, Nat. Phys. **6**, 625 (2010).

[59] J. Petit, D. Rivière, H. Kellay, and J. Delville, Break-up dynamics of fluctuating liquid threads, Proc. Natl. Acad. Sci. USA **109**, 18327 (2012).